



AFRICAN VULTURE OPTIMIZED INTEGRATED CONTROL TECHNIQUE FOR PV FED OPEN-END WINDING INDUCTION MOTOR PUMP APPLICATION

KAVYA VENUGOPALAN¹, JEGATHESAN VARGHESE², JARIN THANKASWAMY³

Keywords: Open-end winding induction motors; Photovoltaic; Scalar coupled pulse with modulation (PWM); African vulture optimization; Dual inverter; Maximum power point tracking (MPPT); Total harmonic distortion (THD).

Open-end winding induction motors (OEWIM) have gained much attention, and they are used for solar photovoltaic (PV) fed pumping applications as a compromise alternative to multi-level inverters. Solar irradiance conditions further exacerbate the nonlinear control problem, resulting in significant loss of power and low reliability, which affects motor operation. To overcome these issues, this paper presents an optimized integrated control technique-based PV integrated three-level dual inverter fed Open-end winding induction motors for pumping application. An integrated African vulture optimization algorithm and scalar coupled pulse width modulation (AVO-SCPWM) based control techniques are proposed to extract the maximum power from the solar PV source and control the induction motor pump. Here, the AVO-based maximum power point tracking (MPPT) technique adjusts the modulation index (m_a) by insolation and temperature. The proposed technique balances the zero-sequence current, reduces THD, and reduces the switching losses over the inverter. The proposed work is evaluated in MATLAB/Simulink software and compared with the existing conventional induction motor (IM), Conventional OEWIM Drive, and scalar decoupled PWM-based IM techniques under two climatic conditions. Thus, the simulation results demonstrate that the proposed technique accomplishes better than the existing techniques.

1. INTRODUCTION

In recent years, due to rapid technological advances, electricity demand has increased, and fuel energy demand has also increased. Apart from demand, power generation using fuel energy sources (coal) results in the production of greenhouse gases such as CO_2 , NO_2 , etc. As a result, the rate of pollution rises. Hence, to overcome this problem, the world is grazing towards producing electricity using renewable energy sources (RES). PV is widely utilized in many applications, such as agriculture, businesses, hydropower plants, and residential buildings. The only difficulty with PV is the lower conversion efficiency [1,2]. Numerous topologies have been adopted to enhance the efficiency of PV. Harvesting maximum power from a PV source is one of the best ways to improve efficiency. Hence, many maximum power extraction algorithms are documented in the literature.

The distributed maximum power point tracking (DMPPT) technique is more appropriate for residential and agricultural pumping systems and industries [3]. Because of non-uniform temperature and insolation at the installation site, a mismatch of array parameters causes variance in the characteristics of PV cells. This scenario has two negative consequences: power loss and decreased reliability. Hence, employing the MPPT approach, which aims to extract determined energy from the PV, is necessary. At first, each PV array is associated with a dc converter to extract supreme power from the PV array. Before connecting this to an inverter, the dc converters are cascaded. It leads to increased costs [4,5].

Developing solar-based water pumping for irrigation is drawing more attention today in rural areas. Solar energy sources have been available for irrigation, but they utilize dc motors. Due to their ongoing maintenance and high cost, dc motors may need to be considered [6]. The brushless dc (BLDC) motor is another replacement choice for a dc motor. Due to their high cost and need for complicated control electronics, BLDC motors may still need to be a viable option for PV pumping systems [6,7]. For a system that pumps water

from solar panels, an induction motor might be a practical and superior option [7]. Most research projects employ traditional induction motors with two or one power conversion stage. In a two-level PV system, a dc-dc converter is used to raise the voltage and aid in maximizing the output of the PV source, and the inverter is employed to supply the motor pump load with the necessary ac power. The alternative solution is the one-stage system using a single inverter [8–10].

An exploration of diverse control strategies for the considered driven system is undertaken. Alternative approaches in the literature include Backstepping control, Sliding mode third-order control, predictive control, and artificial intelligent control. While recognizing this array of control methodologies, the primary focus of this study is on an optimized, integrated control technique tailored for solar PV-fed pumping applications using open-end winding induction motors. The introduction section thus provides a contextual overview of the broader landscape of control strategies, specifically emphasizing the proposed AVO-SCPWM-based control techniques. This strategic approach addresses the intricate challenges of nonlinear control issues exacerbated by solar irradiance conditions, ultimately enhancing system reliability and performance. This study presents a new approach for water pumping using a single-stage solar PV-connected DI-fed open-end winding induction motor drive (OEWIM). Its key advantages include minimizing torque and current ripples, maintaining low total harmonic distortion (THD), and achieving high efficiency. Employing an African vulture optimization (AVO) algorithm and scalar coupled PWM technique MPPT and proficiently drives induction motor pumps. This innovative scheme optimizes solar PV usage while efficiently controlling the connected motor. The detailed contributions are outlined below. A novel optimized, integrated control technique based on solar-powered level DI-fed open-end winding induction motor drive (OEWIM) is designed, and the model of the PV panel is also used.

- A novel African vulture optimization (AVO) based MPPT control method and scalar coupled PWM for

¹ Karunya Institute of Technology and Sciences (Deemed University), Coimbatore, India (Corresponding author)

² Karunya Institute of Technology and Sciences (Deemed University), Coimbatore, India

³ Jyothi Engineering College, Thrissur, Kerala, India

E-mails: kavya@karunya.edu.in, jegathesan@karunya.edu.in, jarint@jecc.ac.in

induction motor control aims to boost motor performance.

- This technique minimizes zero-sequence current, lowers total harmonic distortion (THD), and cuts switching losses in the inverter. MATLAB/Simulink simulations compare their effectiveness against conventional methods like conventional IM and scalar decoupled PWM-based IM.

2. MODELING OF THE PROPOSED SYSTEM

The setup of a solar PV-powered pumping system comprises several components: solar PV arrays, two inverters (designated as inverter 1 and inverter 2), a three-phase open-end winding induction motor integrated with pump loads, and a suggested controller system utilizing AVO-MPPT and SCPWM techniques, as depicted in Fig. 1. Each of these elements will be thoroughly examined in the subsequent subsections for a comprehensive understanding.

2.1. SOLAR PV MODEL

A solar cell is the basic design of a PV array. Figure 2 depicts the mathematical configuration of a PV cell. Numerous PV cells are interconnected to formulate the PV module. The mathematical arrangement of a PV array [11]:

$$I = n_p I_{ph} - n_p I_s \left[\exp\left(\frac{q}{KTA}\right) \left(\frac{V}{n_s}\right) - 1 \right] - n_p I_{rs} \left[\exp\left(\frac{q}{KTA}\right) \left(\frac{V}{n_g}\right) - 1 \right]. \quad (1)$$

Thus, the calculated PV power can be obtained using [12]:

$$P = IV = n_p I_{ph} V \left[\left(\frac{q}{KTA}\right) \frac{V}{n_s} - 1 \right], \quad (2)$$

where I_{ph} is the photocurrent, n_s the series cells, and n_p the parallel cells.

2.2. MODEL OF SYMMETRICAL DUAL INVERTER CONFIGURATION

A dual inverter is formed by combining two, and three-level inverters. Both inverters are coupled to a net voltage of V_{dc} . An input voltage of $V_{dc}/2$ is symmetrically linked to both inverters. This topology prevents the circulation of zero-sequence current in the load [13].

However, the two isolation transformers required to supply the dc source will increase the system's bulkiness and cost. Because the zero-sequence current is not present in this arrangement, lowering common-mode voltage (CMV) should be highlighted.

Table 1

The final pole voltage available in symmetric dual inverter topology				
Effective Pole voltage	Inverter 1 pole voltage	Switches turned ON in inverter 1	Inverter 2 pole voltage	Switches turned ON in inverter 2
$-V_{dc}/3$	0	S_{14} or S_{16} or S_{12}	$V_{dc}/3$	S_{25} or S_{23} or S_{21}
0	0	S_{14} or S_{16} or S_{12}	0	S_{25} or S_{23} or S_{21}
0	$V_{dc}/3$	S_{11} or S_{13} or S_{15}	$V_{dc}/3$	S_{25} or S_{23} or S_{21}
$V_{dc}/3$	$V_{dc}/3$	S_{11} or S_{13} or S_{15}	0	S_{25} or S_{23} or S_{21}

Figure 1 illustrates the pole voltages of inverters 1 and 2 (V_{a0} , V_{b0} , V_{c0}), ($V_{a'0}$, $V_{b'0}$, $V_{c'0}$), respectively. The effective pole and line voltages are also represented. $V_{oo'}$ represents the common mode voltage. When $V_{dc}/2$ is applied to the input, inverter 1 produces a pole voltage of $V_{dc}/2$ and 0, and Inverter 2 about 0 and $V_{dc}/2$. The DI's effective pole voltage for a V_{dc}

input is $(+V_{dc}/2, 0, -V_{dc}/2)$. Because this design generates three voltage levels, we can call it a three-level dual inverter [14,15]. VCMV denotes the common-mode voltage. Table 1 depicts the switching pattern of the inverters and the net pole voltages.

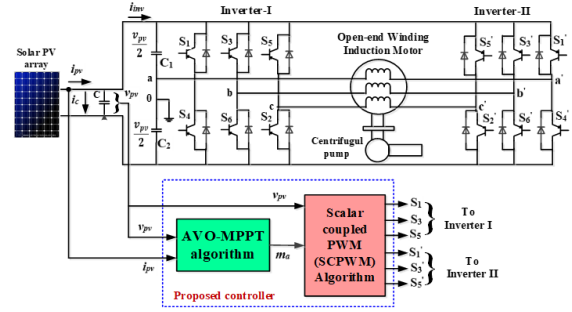


Fig. 1 – Schematic illustration of the planned AVO-SCPWM control.

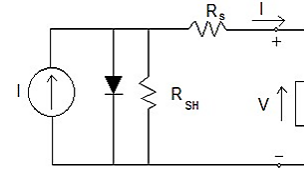


Fig. 2 – Equivalent circuit of PV cell.

$$V^{aa'} = V_{a0} - V_{a'0}, \quad (3)$$

$$V^{bb'} = V_{b0} - V_{b'0}, \quad (4)$$

$$V^{cc'} = V_{c0} - V_{c'0}, \quad (5)$$

$$V_{CMV} = V_{oo'} = \frac{V^{aa'} + V^{bb'} + V^{cc'}}{3}, \quad (6)$$

$V^{aa'}$, $V^{bb'}$, $V^{cc'}$ are the phase voltages of the inverter.

2.3. MODEL OF OPEN-END WINDING INDUCTION MOTOR (OEWM)

Standard three-phase induction motors can transform into open-end winding induction motors by accessing the neutral point [16]. This configuration is called OEWM in vector form, as illustrated below.

$$\begin{cases} \vec{u}_s = R_s \vec{i}_s + p(L_{s\sigma} \vec{i}_s + L_m \vec{i}_g) + j\omega_s (L_{s\sigma} \vec{i}_s + L_m \vec{i}_g) \\ \vec{u}_r = R_r \vec{i}_r + p(L_{r\sigma} \vec{i}_r + L_m \vec{i}_g) + j\omega_f (L_{r\sigma} \vec{i}_r + L_m \vec{i}_g), \\ 0 = R_c \vec{i}_c - pL_m \vec{i}_g - j\omega_s L_m \vec{i}_g \end{cases} \quad (7)$$

where p is a differential operator, and ω_f is the slip angular velocity. The relationship between the current vectors is:

$$\vec{i}_s + \vec{i}_r = \vec{i}_g + \vec{i}_c. \quad (8)$$

The motor's electromagnetic torque (T_e) is denoted by:

$$T_e = -p\psi_r i_t. \quad (9)$$

The rotor's kinematical equation is as follows:

$$pJ_m \omega_m = T_e - (T_l \text{efficiency} + B\omega_m + C). \quad (10)$$

The OW-IM's can then be stated as

$$\begin{cases} \eta_{mot} = T_l \omega_m / (\vec{u}_s \vec{i}_s) \\ \eta_{gen} = (\vec{u}_s \vec{i}_s) / T_l \omega_m \end{cases}. \quad (11)$$

The inverter's ability to share power is primarily determined by the overlapping area of the voltage modulation ranges of the two inverters [17]. The power-sharing ratio of a DI is:

$$P_{inv1} : P_{inv2} : P_m = |\vec{u}_{s1}| : |\vec{u}_{s2}| : |\vec{u}_s|. \quad (12)$$

OEWM's pump drive is described by:

$$T_{em} = J \frac{d\omega_{rm}}{dt} + B\omega_{rm}^2 + T_l, \quad (13)$$

were ω_{rm} is the motor shaft's instantaneous angular velocity (rad/s), B the torque coefficient of centrifugal load, T_l the load torque (Nm), and J the motor's inertia (kg/m²).

3. PROPOSED AVO-SCPWM TECHNIQUE-BASED CONTROL STRATEGY

This research uses an optimized integrated (AVO-SCPWM) control strategy based on a solar PV-driven DI-connected OEWIM pump drive to control the MPPT and motor. Integrated algorithms generate the necessary PWM control signals for 2-level dual-inverters. Figure 3 illustrates the flowchart of the proposed control algorithm. The MPPT technique based on AVO ensures maximum PV power is extracted from the PV source, so the PV is efficiently utilized. Scalar-coupled PWM techniques are used to control inverter pulses. This keeps constant rated flux in the motor, allowing the machine to output its maximum torque for a given PV power. Maintaining the maximum torque in pump drive applications where torque is proportional to speed squared further helps maximize the pump's performance.

3.1. AVO-BASED MPPT CONTROL TECHNIQUE

The AVO method is used in this study to increase the optimization performance of the MPPT controller.

3.1.1. African vulture optimization (AVO) algorithm

The concept behind the African vulture optimization algorithm (AVOA) draws inspiration from the foraging behavior of vultures in search of sustenance. Vultures, predatory birds, seek out injured or weak animals as their prey. This behavior not only aids in their survival but also helps prevent the spread of infectious diseases by scavenging on carcasses. In the context of the algorithm simulating the search for food for a group of N vultures, these birds are divided into two distinct groups.

Each vulture group possesses different capabilities in seeking food, allowing the algorithm to identify the optimal solution and a secondary alternative that can substitute for one of them. The formulation stage is considered the weakest and most starved phase for the vultures oriented toward combating hunger. Consequently, the algorithm tends to discover the best solutions further away from this group [18,19].

(i) Initial Stage

Parameters for each search agent's solution are expressed as

$$Position = \text{rand}(N, 1) * (ub - lb) + lb \quad (14)$$

where lb is the lower bound, ub is the upper bound, N is the vulture population, and rand is the random value range of [0,1].

(ii) Fitness calculation

Each iteration includes a fitness calculation for each vulture, resulting in the optimal solution for the first vultures and the best solution for the second group. Based on the probability eq (30) using the Roulette wheel, the best solution is obtained in the range of [0,1] for each group.

$$P_i = \frac{F_i}{\sum_{i=1}^n F_i} \quad (15)$$

(iii) Behavior of vultures

Hungry vultures are the frailest; thus, it seeks food near the toughest and is violent since their power is insufficient to conduct a far adequate search with a z value less than 0

$$F = (2 * \text{rand}_1 + 1)q \left(1 - \frac{k}{\text{iter}_{max}} \right) + r \left(\sin \left(\frac{\pi}{2} * \frac{k}{\text{iter}_{max}} \right) + \cos \left(\frac{\pi}{2} * \frac{k}{\text{iter}_{max}} \right) - 1 \right), \quad (16)$$

where rand_1 is the random number in the [0,1] range, iter_{max} maximum iteration, F is not a hungry vulture, q and r are

random numbers within the range of [-1,1] and [-2,2], respectively, and k is the iteration number. With the second portion of the equation, this algorithm evades optimal local convergence and is more reliable. As F increases, the vulture explores other regions for the solution, while as F decreases, it arrives at the exploitation phase, aiming to improve the solution's quality [20,21].

(iv) Exploration phase

Equation (17) indicates that the vulture's search is near to one of the best solutions discovered when $\text{rand}_{p1} >= p1$. Equation (18) indicates that vultures seek a new remote area of the area when $\text{rand}_{p1} < p1$.

$$k(i+1) = R(i) - F + \text{rand}_2 * (ub - lb) * \text{rand}_3 + lb, \quad (17)$$

$$k(i+1) = R(i) - (|XR(i) - k(i)|F), \quad (18)$$

where $k(i)$ is the current iteration vulture location, $k(i+1)$ the preceding iteration vulture location, $R(i)$ the top solution.

(v) Exploitation phase

There are two stages to the Exploitation phase. One of the techniques in each step is chosen using the characteristics $p2$ and $p3$, which have values in the range [0,1]. Two methods to the initial stage are rotating flight and siege fight. The consequence of rotational flight is as follows;

$$k(i+1) = R(i) - \left(\left(R(i) * \frac{\text{rand}_5 * k(i)}{2\pi} * \cos k(i) \right) + \left(R(i) * \frac{\text{rand}_6 * k(i)}{2\pi} * \sin k(i) \right) \right). \quad (19)$$

According to parameter $p3$, the second exploitation phase involves food competition, presenting itself as either an intense siege-like scenario or resembling the gathering of diverse vultures around a food source. When the randomly generated value rand_{p3} is greater than or equal to $p3$, eq. (20) demonstrates that vultures gather around the food source. Conversely, if $p3$ exceeds rand_{p3} , eq. (21) illustrates a situation of aggressive competition among the vultures for the food source.

$$k(i+1) = \frac{M_1 + M_2}{2}, \quad (20)$$

$$k(i+1) = R(i) - |d * F * LF|, \quad (21)$$

where $d = R(i) - k(i)$ it is the distance between the vulture and the two groups' finest vultures, F is calculated using eq. (16), M_1 & M_2 the motion of vulture, and LF - Lévy flight pattern. The SCPWM algorithm then employs the best duty cycle value determined to control the DI coupled to the OEWIM fed pump, which can obtain the extreme available power from the PV resource shown in Fig. 3.

PV array voltage instantaneous values (V_{pv}), and PV current (I_{pv}), are given in the MPPT algorithm in the MPPT section. The PV power (P_{pv}) is then determined using the AVO algorithm's averaged values of V_{pv} and I_{pv} . The optimal value is then determined by analyzing the current PV voltage and power to previously accessible values. This modulation index, m_a ($m_a = m_a \pm \Delta m_a$) values, which can be used to regulate the operating voltages of PV sources or to track MPP for PV sources separately. Furthermore, the Scalar coupled PWM approach uses the m_a to determine the common frequency of the modulating wave.

3.2. Scalar couple PWM (SCPWM) technique motor control

PWM pulses are produced in the coupled technique by addressing both inverters in a coupled way. In other words, switching pulses for the 2 inverters are created by combining three-level pulses. To generate a three-level output voltage,

27 switching states are required. Figure 4 depicts the 27 switching states of a 3-level inverter along a dq axis plane. As a result, this topology decreases the difficulty of selecting switching states.

The reference signal provided by this topology is as follows

$$V_a = V_m \cos(\omega t), \quad (22)$$

$$V_b = V_m \cos(\omega t - 2\pi/3), \quad (23)$$

$$V_c = V_m \cos(\omega t - 4\pi/3). \quad (24)$$

Figure 5 shows that a zero-sequence signal is added to the reference signal and enhances the quality of the output current and voltage. In addition, however, significantly reduces harmonic distortion.

$$V_i^* = V_i + V_{zs}, \quad i = a, b, c, \quad (25)$$

$$V_{zs} = \frac{V_{dc}}{2}(2a_0 - 1) - a_0 V_{max} + (a_0 - 1)V_{min}. \quad (26)$$

Here, V_{max} and V_{min} are the instantaneous values of the reference signals, V_{dc} the input voltage, and a_0 a constant (0 to 1).

Different modulating signals can be generated by altering the value of ' a_0 .' This defines whether the operation is continuous or discontinuous. As a result of selecting a_0 value with these conditions $V_{max} + V_{min} < 0$, then $a_0 = 0$, else $a_0 = 1$. At $a_0 = 0.5$, it operates in continuous mode.

By providing the highest torque possible under varying environmental conditions, the OEWM pump drive could perform more efficiently.

4. RESULTS AND DISCUSSIONS

The proposed AVO-SCPWM control-based system performance is investigated using MATLAB/Simulink software. The proposed AVO-SCPWM technique-based IM drive system is compared with the existing techniques such as conventional IM, OEWM drive, and scalar decoupled PWM-based IM. The single-stage PV-powered dual inverter fed OEWM drive for pump application is considered for simulation. A 220 V supply is provided to inverters 1 and 2, resulting in a dc input voltage of 540 V, and the f_s is 3 kHz for the proposed dual inverter arrangement. The proposed scheme is simulated for various insolation levels and ambient temperatures to demonstrate performance under all dynamic conditions.

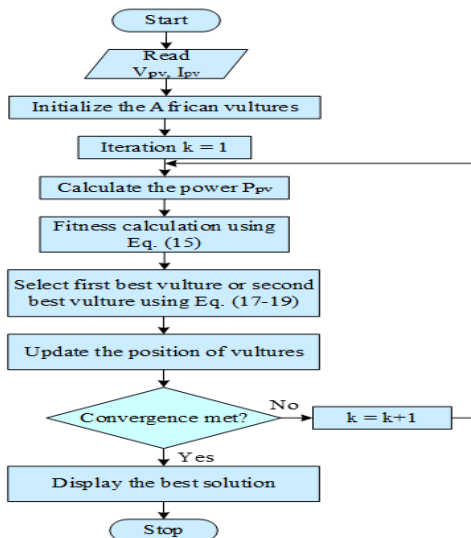


Fig. 3 – Proposed AVO-based MPPT technique.

Case 1: Under constant solar irradiation.

Case 2: Under varying solar irradiation.

In this case, the designed PV array delivers 500 W at 1000 W/m² solar radiation. Figure 6 depicts the voltage and power output simulation results using the proposed AVO-SCPWM method. By observing the waveforms of PV power and m_a , it is possible to observe that PV power increases and decreases with insolation (G) and temperature (T).

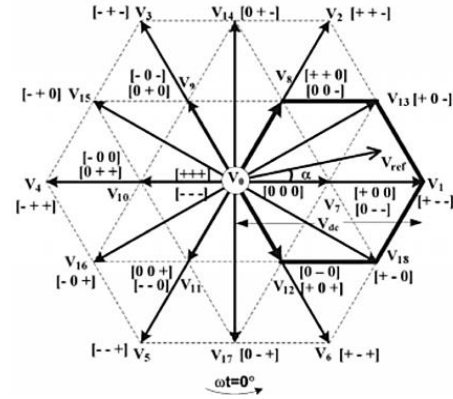


Fig. 4 – Three-level switching states of a coupled inverter.

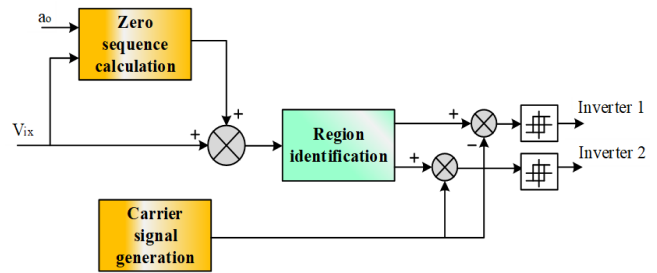


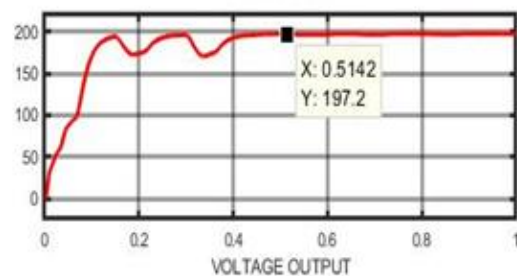
Fig. 5 – Scalar-coupled PWM-based dual inverter configuration.

4.1. ANALYSIS OF CASE 1

The maximum power can be tracked directly by applying AVO-MPPT directly to constant irradiation levels. It is proposed that the proposed method reduces the oscillations of the output power around the MPP. The African vulture, therefore, searches a nonlinear space region to control its output voltage. According to the findings, the AVO algorithm converges swiftly and reaches the best culture position in seconds. Additionally, it is noted that the AVO algorithm produces higher output voltage and power from the PV module than the other method, reaching the steady-state value more quickly. The inverter and motor characteristic under a constant radiation setting is shown in Fig. 7.

4.2. ANALYSIS OF CASE 2

MPPT approaches struggle in dynamic climates, causing slow response times (0.25...0.75 s). PV voltage and power are monitored across irradiation levels, reducing by 10...90 %.



(a)

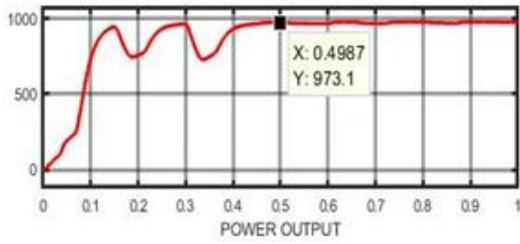
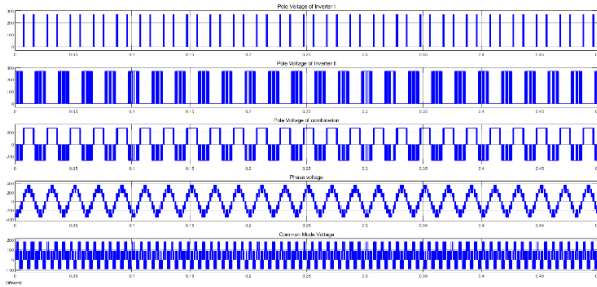
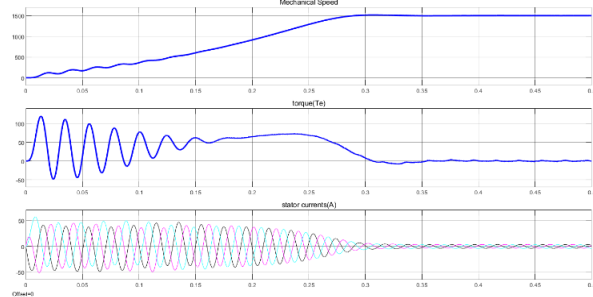


Fig. 6 – Performance of case 1: a) PV voltage; b) PV power.



(a)



(b)

Fig. 7 – Proposed system performance of: a) inverter output; b) motor output at case 1.

Figure 8 justifies this, matching highest power values during variant tracking and near MPP. PV voltage waveform shows quick increase and fall with insolation changes. Highest power is obtained with recommended topology.

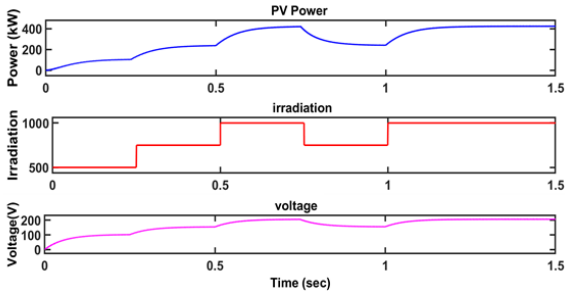
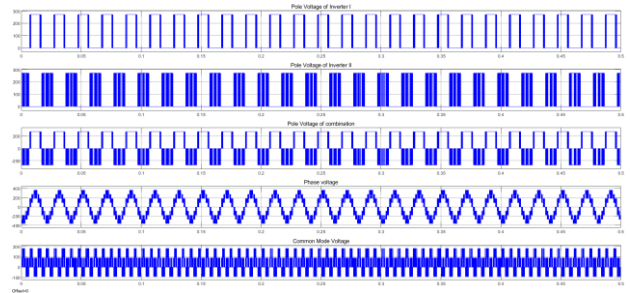
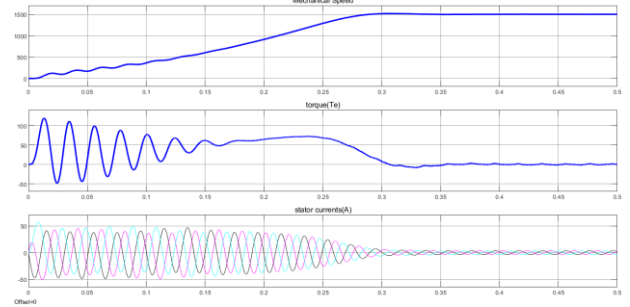


Fig. 8 – Performance of: a) PV power; b) irradiance; c) voltage.

Variations in PV array voltage impact motor phase voltage across climates. Power extraction from PVs precedes motor shaft power extraction. Motor slip rises with sudden insolation, and temperature drops, reducing power output. PV power declines significantly as the PV source operates at the present source under these conditions. The algorithm functioned well despite worst-case scenarios, stabilizing the system within seconds. Constant PV and motor parameters ensure stability despite changing environmental conditions in simulations, exaggerating real-life scenarios. Figure 9 displays motor side waveforms. Optimal torque occurs at ma between 0.8 and 1, stabilizing between 0.5 and 0.9.



(a)



(b)

Fig. 9 – Proposed system performance of (a) inverter output (b) motor output at case 2.

The developed MPPT algorithm's efficacy is confirmed by a low ripple in PV power and relates with peak PV power at constant and varied. Furthermore, the ripple value of the current is higher throughout lower insolation, and the THD decreases as insolation increases. In summary, as PV power increases, system performance improves. Table 2 provides a summary of the simulation results, illustrating this observation.

Table 2

Simulation results of proposed AVO-SCPWM

G	T	PV	Output	η	Torque	Speed	Current
Su	(°C)	power	power	(%)	ue	(rpm)	THD
ns		(W)	(W)		(Nm)		(%)
0.1	25	329	240	72.9	6.5	352	11.9
0.3	30	1040	895	85.9	11.59	740	8.59
0.5	40	1717	1528	88.99	14.1	1036	15.3
0.7	45	2406	2157	89.09	17.9	1161	8.88
0.9	50	3072	2735	89.65	21.98	1187	4.52
1	55	3365	2990	90.01	24.25	1230	3.66

Table 3

Comparison of THD with different topologies

Topology	Voltage (THD)	Current (THD)
Conventional IM	93.66	13.69
Conventional OEWIM Drive	64.36	12.56
Scalar Decoupled PWM-based IM	59.23	10.29
Proposed technique	32.45	3.66

Table 4

Comparison of various control strategies

Control Strategy	Overshoot (%)	Rise & Settling Time (sec)	Power error (%)	Steady State Error (%)
PSO [5,6]	2.1	0.1 & 0.4	10	1.1
Sliding control	1.8	0.15 & 0.5	12	0.9
[7] PI	2.6	0.1 & 0.45	15	0.9
[8] PI	2.8	0.1 & 0.48	15	0.9
[18]	1.21	0.08 & 0.15	8	0.5
African vulture Optimization	1.20	0.09 & 0.18	8	0.5
proposed	0.05	0.01 & 0.1	5	0.1

Comparative analysis reveals lower THD in the AVO-SCPWM technique than conventional IM, conventional OEWIM drive, and scalar decoupled PWM-based IM, reducing current THD and copper losses, optimizing energy efficiency, and enhancing PV-based induction motor efficiency. Simulation results confirm effectiveness, suggesting AVO-SCPWM's utility for PV water pumping. Table 4 presents a comprehensive overview by comparing various control strategies employed in the solar PV-fed pumping system utilizing (OEWIM). This table serves as a visual representation and a succinct summary of the diverse control strategies under scrutiny, highlighting their respective performances in response to the dynamic conditions associated with solar irradiance and environmental temperature variations.

6. CONCLUSION

This paper introduces a solar PV-fed dual inverter connected to an OEWIM for a pump application system. A scalar-based coupled PWM technique, integrated with the MPPT algorithm, controls the motor effectively. Using MATLAB/Simulink, the proposed AVO-SCPWM control-based OEWIM system is compared with existing techniques in two climatic scenarios. Simulation results show that AVO-SCPWM significantly balances zero-sequence current, reduces harmonics (3.66 %), minimizes ripple content in current THD, and lowers inverter switching losses. This robust control algorithm ensures system stability, even in challenging conditions, making PV power-fed water pumps a viable solution. Future research aims to expand control techniques for solar PV sources, enhancing adaptability and efficiency. This includes extending applications to various PV sources, incorporating efficient management strategies, and exploring advanced control algorithms and optimization techniques. Our commitment to innovation in Solar PV-fed pumping applications drives these envisioned future works and perspectives.

ACKNOWLEDGEMENTS

The author would like to express his heartfelt gratitude to the supervisor for his guidance and unwavering support during this research for his guidance and support.

Received on 13 December 2023

REFERENCES

1. B. Mountain, P. Szuster, *Solar, solar everywhere: opportunities and challenges for Australia's rooftop PV systems*, IEEE Power Energy Mag., **13**, 4, pp. 53–60 (2015).
2. A.A.A. Radwan, Y.A.R.I. Mohamed, *Power synchronization control for grid-connected current-source inverter-based photovoltaic systems*, IEEE Trans. Energy Conv., **31**, 3, pp. 1023–1036 (2016).
3. M.A. Elgendy, B. Zahawi, D.J. Atkinson, *Operating characteristics of the P&O algorithm at high perturbation frequencies for standalone PV systems*, IEEE Trans. Energy Conv., **30**, 1, pp. 189–198 (2015).
4. A. Costabeber, M. Carraro, M. Zigliotto, *Convergence analysis and tuning of a sliding-mode ripple-correlation MPPT*, IEEE Trans. Energy Conv., **30**, 2, pp. 696–706 (2015).
5. U.K. Kalla, N. Bhati, K. Chariya, I. Qureshi, *Design and analysis of solar PV fed IMD water-pumping system*, 2021 International Conference on Sustainable Energy and Future Electric Transportation (SEFET), IEEE, pp. 1–6 (2021).
6. Y. Jiang, J.A.A. Qahouq, M. Orabi, *Ac PV solar system distributed architecture with maximum power point tracking*, Proc. IEEE International Telecommunications Energy Conference (IEEE-INTLEC'12), Scottsdale (AZ), USA, 2012.
7. S. Jain, A.K. Thopukara, R. Karampuri, V.T. Somasekhar, *A single-stage photovoltaic system for a dual inverter-fed open-end winding induction motor drive for pumping applications*, IEEE Trans. Power Electron., **30**, 9, pp. 4809–4818 (2015).
8. M.W. Shah, R.L. Biate, *Design and simulation of solar PV model using MATLAB/Simulink*, International Journal of Scientific & Engineering Research, **7**, 3, pp. 551–554 (2021).
9. T. Ma, H. Yang, L. Lu, *Solar photovoltaic system modeling and performance prediction*, Renewable and Sustainable Energy Reviews, **36**, pp. 304–315 (2014).
10. S. Jain, A.K. Thopukara, R. Karampuri, V.T. Somasekhar, *A single-stage photovoltaic system for a dual-inverter-fed open-end winding induction motor drive for pumping applications*, IEEE Trans. on power Electronics, **30**, 9, pp. 4809–4818 (2014).
11. J. Korhonen, J. Honkanen, T.J. Kärkkäinen, J. Nerg, P. Silventoinen, *Modulation and control methods to reduce zero sequence current in open-end winding motors*, 2017 IEEE International Electric Machines and Drives Conference (IEMDC), IEEE, pp. 1–6 (2017).
12. G.A. Ghazi, H.M. Hasanien, E.A. Al-Ammar, R.A. Turkey, W. Ko, S. Park, H.J. Choi, *African vulture optimization algorithm-based pi controllers for performance enhancement of hybrid renewable-energy systems*, Sustainability, **14**, 13, pp. 8172 (2022).
13. A. Hossam-Eldin, H. Mostafa, H. Koth, K.M. AboRas, A. Selim, S. Kamel, *Improving the frequency response of hybrid microgrid under renewable sources' uncertainties using a robust lfc-based African vulture optimization algorithm*, Processes, **10**, 11, pp. 2320 (2022).
14. D. Benoudjit, S. Rid, N. Nait-Said, M. Saidnait-Said, L. Chrifi-Alaoui, *Electric vehicle propelled by dual-induction motors structure: experimental results*, Rev. Roum. Sci. Techn. – Électrotechn. et Énerg., **68**, 2, pp. 170–175 (2023).
15. R. Sheeja, R. Nishant, *Reduction in greenhouse gas emission by using sustainable transportation systems to increase the environmental and economic benefits*, International Journal of System Design and Computing, **01**, 01, pp. 18–25 (2023).
16. B. Sivasankari, M. Shunmugathammal, A. Appathurai, and M. Kavitha, *High-throughput and power-efficient convolutional neural network using one-pass processing elements*, Journal of Circuits, Systems and Computers, **31**, 13, pp. 225–226 (2022).
17. E.G. Boudissa, F. Habbi, M. Bounekhla, N. Dif, *A memetic algorithm applied to induction machine parameters identification based on an output error: memetic algorithm for induction machine identification*, Rev. Roum. Sci. Techn. – Électrotechn. et Énerg., **68**, 3, pp. 266–270 (2023).
18. K.K. Kumar, M.W. Iruthayarajan, A.S. Kamaraja, *Investigation of a solar incorporated improved quasi-Y-source dc-dc step-up converter connected with phase-shifted converter in electric vehicle battery charging*, Electr. Eng., **105**, pp. 3647–3667 (2023).
19. P. Deepa, S. Rajakumar, P.J. Shermila, E.A. Devi, M.E. Prince, A.J.G. Malar, *New hybrid Cuk-Landsman high gain dc-dc converter modelling and analysis*, Power, **9**, 8, pp. 8–16 (2022).
20. A. Agasthian, R. Pamula, L.A. Kumaraswamidhas, *Integration of monitoring and security based deep learning network for wind turbine system*, International Journal of System Design and Computing, **01**, 01, pp. 11–17 (2023).
21. S.V. Lakshmi, M.A. Rejula, K. Sujatha, A. Ahilan, *Recognition of brain stroke shape using multiscale morphological image processing*, The Imaging Science Journal, **69**, (1-4), pp. 28–37 (2021).